J Solid State Eletrochem (2003) 8: 2–6
DOI 10.1007/s10008-003-0415-7

ORIGINAL PAPER

Martin Kalbáč · Markéta Zukalová · Ladislav Kavan

Phase-pure nanocrystalline $Li_4Ti_5O_{12}$ for a lithium-ion battery

Received: 15 November 2002 / Accepted: 11 June 2003 / Published online: 13 September 2003

Abstract Phase-pure nanocrystalline $Li_4Ti_5O_{12}$ with BET surface areas between 183 and 196 m^2/g was prepared via an improved synthetic protocol from lithium ethoxide and titanium(IV) butoxide. The phase purity was proved by X-ray powder diffraction, Raman spectroscopy and cyclic voltammetry. Thin-film electrodes were prepared from two nanocrystalline samples of $Li_4Ti_5O_{12}$ and one microcrystalline commercial sample. Li-insertion behavior of these electrodes was related to the particle size.

Keywords $Li_4Ti_5O_{12}$ · Lithium insertion · Nanocrystalline materials · Phase purity · Spinel

Introduction

$Li_4Ti_5O_{12}$ (spinel) was introduced in the early 1990s as a promising "zero-strain" Li-insertion host [1, 2, 3]. It accommodates three Li^+ per formula unit with a theoretical capacity of 175 mAh/g:

$$Li_4Ti_5O_{12} + 3e^- + 3Li^+ \rightarrow Li_7Ti_5O_{12} \quad (1)$$

The spinel $Li_4Ti_5O_{12}$ is conveniently prepared by a solid-state reaction of TiO_2 and Li_2CO_3 or LiOH at 800–1000 °C [1, 2, 4, 5, 6, 7, 8, 9, 10, 11]. This synthetic route primarily yields micron-sized crystals [11]. There has been one report on "nanocrystalline" $Li_4Ti_5O_{12}$ resulting from the high-temperature reaction of TiO_2 and Li_2CO_3 [12], but neither the particle size nor preparative details were specified. The "nanosized" $Li_4Ti_5O_{12}$ offered at least a 30% improvement in rate capability at 1–10 C in a hybrid cell with a supercapacitor-like counter-electrode [12, 13]. This conclusion agrees with previous reports on TiO_2 (anatase), in which the charge capability also improved if the host material had nanocrystalline morphology [14, 15, 16].

Nanocrystalline $Li_4Ti_5O_{12}$ (spinel) with a crystal size of 30 nm was prepared by hydrothermal reaction of TiO_2 and LiOH at 130–200 °C [17]. There have been several attempts to grow nanocrystalline $Li_4Ti_5O_{12}$ (spinel) by the sol-gel method from lithium acetate and titanium(IV) isopropoxide [18, 19] or butoxide [20]. In both cases, calcination at 800 °C was necessary to obtain a reasonably pure spinel phase [19] and to improve the electrochemical performance [20]. The sol-gel product from the butoxide route exhibited a grain size of ca. 100 nm, but contained also some rutile impurities [20]. Its Li-insertion capacity was reported to be 272 mAh/g, but the charging reversibility was not tested [20]. This casts doubt on this unrealistic charge capacity. The sol-gel spinel showed considerable capacity fading during the initial 20 cycles [19], which contrasted with the high cycle-life of materials made by solid-state reactions [3, 12]. Nanocrystalline $Li_4Ti_5O_{12}$ spinels with the smallest particle sizes (9–19 nm) were prepared via hydrolytic conversion of a mixture of Li alkoxide and Ti(IV) alkoxide [21]. The product contained 0.3–0.6% anatase and exhibited excellent charge capability in thin-film electrodes [21]. This paper is aimed at further investigation and optimization of this material.

Presented at the 3rd International Meeting on Advanced Batteries and Accumulators, 16–20 June 2002, Brno, Czech Republic

M. Kalbáč · M. Zukalová · L. Kavan (✉)
J. Heyrovský Institute of Physical Chemistry,
Academy of Sciences of the Czech Republic,
Dolejškova 3, 182 23 Prague 8, Czech Republic
E-mail: kavan@jh-inst.cas.cz
Tel.: +420-2-66053975
Fax: +420-2-86582307

Experimental

Preparation of electrodes

The sol-gel synthesis of nanocrystalline $Li_4Ti_5O_{12}$ from Li/Ti alkoxides was described previously [21]. Here, this synthetic protocol was optimized with the aim to achieve the best phase purity, while still keeping the small particle sizes. The final synthetic protocol

towards phase-pure nanocrystalline $Li_4Ti_5O_{12}$ was as follows. Under an argon atmosphere, a 0.9 M solution of LiOEt (Aldrich) in absolute ethanol was mixed with titanium(IV) butoxide (Aldrich) in a stoichiometric molar ratio of Li/Ti = 4:5. The clear yellowish solution was hydrolyzed with a 4 wt% aqueous solution of poly(ethylene glycol) (PEG, $M = 20{,}000$; Aldrich). The amount of PEG corresponded to 150 wt% of the weight of the stoichiometrically expected for $Li_4Ti_5O_{12}$. The mixture was stirred overnight and then evaporated on a rotary evaporator at 40 °C to the consistence of a viscous slurry. This was finally fired at 500 °C under a proprietary calcination program, which was crucial for minimizing the trace anatase impurities.

The hydrothermally processed samples were prepared as follows. The ethanolic solution of Li/Ti alkoxides was hydrolyzed with water, the mixture was stirred overnight, and then evaporated in vacuum at 40 °C. The resulting viscous slurry was autoclaved at 150 °C for 16 h and then mixed with 150 wt% of PEG ($M = 20{,}000$) and annealed at 500 °C as in the previous case. A commercial $Li_4Ti_5O_{12}$ (LT-2 from Titan Kogyo, Japan, 3.1 m^2/g) was also tested for comparison.

Thin-film electrodes from $Li_4Ti_5O_{12}$ were prepared as follows [14, 21]: 0.185 g of the powder precursor was mortared under slow addition of 4×0.06 mL of a 10% aqueous solution of acetylacetone. The mixture was diluted by 0.15 mL H_2O and mixed with 0.13 mL of a 4% aqueous solution of hydroxypropylcellulose (Aldrich, MW 100,000) and 0.03 mL of a 10% aqueous solution of Triton-X100 (Fluka). The obtained slurry was deposited on a sheet of conducting glass (F-doped SnO_2, TEC 8 from Libbey-Owens-Ford, 8 Ω/square) using a doctor-blading technique [14, 21]. The film thickness was adjusted by Scotch tape at the edges of the support, which also allowed making electrical contacts to the electrode. The film was finally calcined for 30 min in air at 450 °C.

Alternatively, the nanocrystalline thin-film electrodes were also prepared directly via doctor-blading and calcination of the primary slurry resulting from the sol-gel synthesis (see above). The geometric area of the $Li_4Ti_5O_{12}$ film was 0.2 cm^2. In some cases the film's area was cut down by mechanical scraping of the film's edges by a piece of glass. This served to finely adjust the charge capacity to a comparable uniform value of ca. 300 mC per electrode.

Methods

The BET surface areas were determined from nitrogen adsorption isotherms at 77 K (ASAP 2010, Micromeritics). Scanning electron microscopy (SEM) images were obtained by a Hitachi S-4700 apparatus. Transmission electron microscopy (TEM) images were obtained by a Philips EM430T microscope operating with a LaB_6 cathode at 300 kV. Powder X-ray diffractometry (XRD) was studied on a Siemens D-5000 diffractometer using Cu Kα radiation. Raman spectra were excited at 2.41 eV (2 mW) by an Ar^+ laser (Innova 305, Coherent) and recorded on a T-64000 spectrometer (Instruments, SA).

Electrochemical measurements were carried out in a one-compartment cell using an Autolab Pgstat-30 (Ecochemie) controlled by GPES-4 software. The reference and auxiliary electrodes were from Li metal; hence potentials are referred to the Li/Li^+ (1 M) reference electrode. $LiN(CF_3SO_2)_2$ (Fluorad HQ 115 from 3M) was dried at 130 °C/1 mPa. Ethylene carbonate (EC) and 1,2-dimethoxyethane (DME) were dried over 4A molecular sieve (Union Carbide). The electrolyte solution, 1 M $LiN(CF_3SO_2)_2$ + EC/DME (1:1 by mass) contained 10–15 ppm H_2O, as determined by Karl Fischer titration (Metrohm 684 coulometer). All operations were carried in a glove box under argon (containing typically 1–5 ppm of O_2 and H_2O).

Results and discussion

Figure 1 shows that our nanocrystalline $Li_4Ti_5O_{12}$ is reasonably monodisperse in mesoscopic dimensions. The TEM pattern (Fig. 1B) evidences that the particles are single crystals with a typical size of ca. 10 nm. The single-crystalline nature of the particles is confirmed by uniform fringes of the cubic lattice. One illustrative example of a relatively large single-crystal particle is highlighted in Fig. 1B. However, by inspecting at high resolution, these fringes are omnipresent in the TEM patterns, showing that the crystals are statistically oriented in the sintered film.

The BET surface areas, S_{BET}, of the as-prepared nanocrystalline materials were 183–196 m^2/g for samples of different batches. If we approximate the morphology by spherical particles of a density of $\rho = 3.5$ g/cm^3, the corresponding particles size, d, can be estimated as [21]:

$$d = 6/\rho S_{BET} \tag{2}$$

Equation 2 gives $d \approx 9$ nm for the found surface areas (183–196 m^2/g), which agrees with the morphology seen by SEM/TEM (Fig. 1). The surface area of the hydrothermally grown material was $S_{BET} = 140$ m^2/g. This translates into $d \approx 12$ nm. Apparently, the increase in particle size is due to Ostwald ripening at hydrothermal recrystallization [21]. The particle growth could be also visualized by comparison of SEM/TEM images of

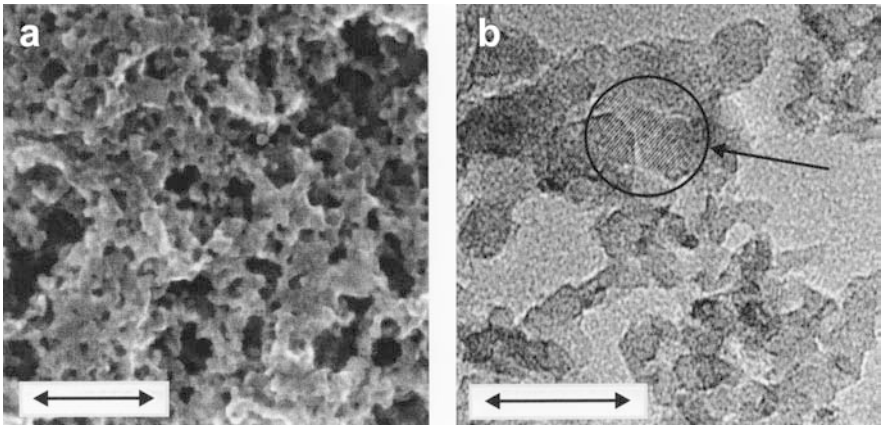

Fig. 1 (**a**) SEM image of as-received (non-autoclaved) nanocrystalline $Li_4Ti_5O_{12}$; scale bar 100 nm. (**b**) TEM image of the same material; scale bar 20 nm. *Highlighted* is one large particle exhibiting well-distinguished fringes of a cubic lattice

autoclaved and non-autoclaved (Fig. 1) materials, but the changes in actual morphologies were not that expressive to demonstrate the expected particle growth ($9 \rightarrow 12$ nm) because of the spread of particle sizes of the real materials. The calculated (Eq. 2) particle size for the commercial LT-2 sample ($S_{BET} = 3.1$ m^2/g) equals 0.6 μm. In this case, the SEM pattern presents clearly distinct particles of ca. 1 μm in size (cf. fig. 1B in [21]).

Powder X-ray diffraction confirms the phase purity of our nanocrystalline spinel (Fig. 2). A careful phase analysis is important, since TiO_2 impurities (anatase, rutile) have been frequently observed in various $Li_4Ti_5O_{12}$ (spinel) materials made by sol-gel methods [19, 20, 21]. Our previous study [21] also pointed at TiO_2 anatase impurity (0.3–0.6 wt%) found in most products from the sol-gel synthesis employing Li/Ti alkoxides. Figure 2 compares the powder diffraction patterns of two typical examples of our materials (nanocrystalline as-received and hydrothermally grown spinel) with the commercial micron-sized product, LT-2. All patterns can be indexed for a cubic lattice of $Li_4Ti_5O_{12}$, while no signs of additional phases are apparent (anatase at $2\Theta \approx 25°$ and rutile at $2\Theta \approx 27°$). The commercial sample LT-2 showed, besides the main line of (400) diffraction at $2\Theta = 43.22°$, also a satellite line at 43.34°, whose assignment is not clear.

The shift of diffraction peaks in Fig. 2 shows that the lattice constant depends on the synthetic protocol. The calculated lattice constants were as follows: 0.8275 nm (nanocrystalline spinel), 0.8366 nm (hydrothermally grown nanocrystalline spinel) and 0.8369 nm (LT-2). The latter value matches well the lattice constant of $Li_4Ti_5O_{12}$ made by high-temperature syntheses: 0.8367 [1], 0.8365 [3], 0.8358 [7] and 0.8357 [6]. The value is also similar to the lattice constant of 0.8359 nm calculated from the JCP2 CAT pattern (PDF number 26-1198). Apparently, the hydrothermally grown material shows the ''normal'' value of the lattice constant, whereas the as-received (non-autoclaved) nanocrystalline spinel exhibits a significantly smaller constant. This conclusion matches our previous report on the sol-gel synthesis of nanocrystalline $Li_4Ti_5O_{12}$ containing small anatase contamination [21].

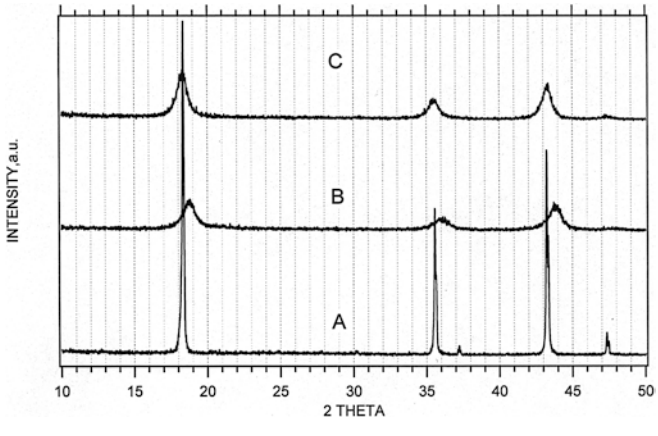

Fig. 2 Powder X-ray diffractogram of (*A*) a commercial $Li_4Ti_5O_{12}$ spinel (LT-2), (*B*) nanocrystalline $Li_4Ti_5O_{12}$ made by the synthetic procedure without hydrothermal treatment, and (*C*) hydrothermally grown nanocrystalline $Li_4Ti_5O_{12}$

The crystallite size d_c (coherent length of the crystal lattice) was approximated from the X-ray line width (w) according to the Scherrer formula:

$$d_c = 0.9\lambda / w \cos\Theta \qquad (3)$$

where λ is the X-ray wavelength (0.1540562 nm) and Θ is the diffraction angle. Equation 3 gives $d_c \approx 9$ nm for the as-received (non-autoclaved) material and $d_c \approx 12$ nm for the corresponding hydrothermally grown material. These particles sizes agree surprisingly well with the particle size calculated from the BET area (Eq. 2).

The phase purity of our nanocrystalline $Li_4Ti_5O_{12}$ is also confirmed by Raman spectroscopy. This method is, reportedly, more sensitive to detect anatase impurities, even in samples which appear to be ''X-ray amorphous'' [22]. Figure 3 shows that our nanocrystalline spinels passed successfully this test also. It does not show any Raman band at 144 cm^{-1}, where the strongest line of anatase is expected to take place (cf. spectra C and B in Fig. 3). Also, rutile would have a peak here (143 cm^{-1}). The spectrum of our nanocrystalline spinel also matches well that of the commercial LT-2 material.

A third proof of the phase purity of our nanocrystalline spinel follows from the cyclic voltammogram of Li insertion (Fig. 4). The positions of the voltammetric peaks (1.51 V for Li insertion and 1.60 V for Li extraction) correspond to the formal potential of $Li_4Ti_5O_{12}$ spinel (cf. Eq. 1), which is reported to be 1.56 V vs. Li/Li$^+$ [1, 8]. The voltammogram confirms that our material is free from anatase, which would manifest itself by distinguished Li-insertion peaks at 1.75 V and 2.0 V vs. Li/Li$^+$ [21]. We have previously shown that the electrochemical detection of anatase is very sensitive and superior to X-ray diffraction for the spinel/anatase mixtures [21].

Hence, in this work, we present an optimized synthetic procedure which allowed us to prepare TiO_2-free spinel reproducibly. Our materials are unique, not only from the point of view of the smallest ever reported particle size (the largest S_{BET}), but also from the point of view of the phase purity, which was confirmed by three independent methods (X-ray diffraction, Raman spectroscopy and electrochemistry).

Figure 5 shows a series of galvanostatic charge/discharge cycles of electrodes prepared from nanocrystalline and commercial micron-sized material (LT-2) at charging rates of 2, 20, 50, 100 and 150 C. The maximum reversible Li-insertion capacity determined from the 2 C cycle (and/or from slow cyclic voltammetry, cf. Fig. 4) was around 300 mC for all three samples. Fast charging is always reversible, but the nanocrystalline electrodes show considerable irreversibility at 2 C. This is apparently due to breakdown processes in the

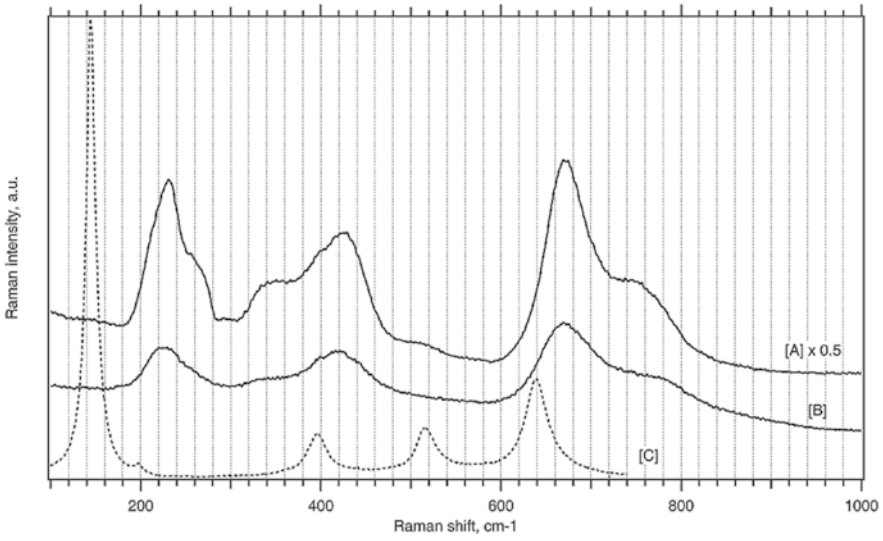

Fig. 3 Raman spectra of (*A*) the commercial micron-sized spinel LT-2, (*B*) a non-autoclaved nanocrystalline spinel, and (*C*) nanocrystalline anatase C200. The latter sample was available from the previous work [14]. The spectra are offset for clarity; the intensity scale is comparable for samples *B* and *C* but is reduced by one half for sample *A*

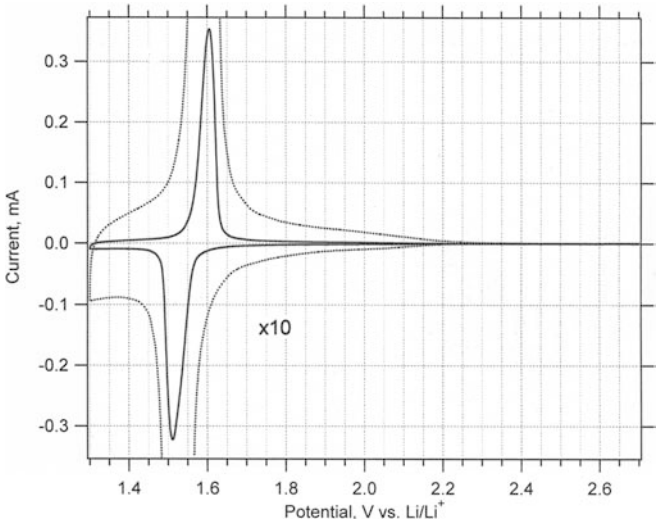

Fig. 4 Typical cyclic voltammogram of phase-pure nanocrystalline $Li_4Ti_5O_{12}$. Electrolyte solution: 1 M $LiN(CF_3SO_2)_2$ + EC/DME (1:1 by mass); scan rate 0.2 mV/s. The *dashed curve* displays the same plot, but with the current scale expanded by a factor of 10

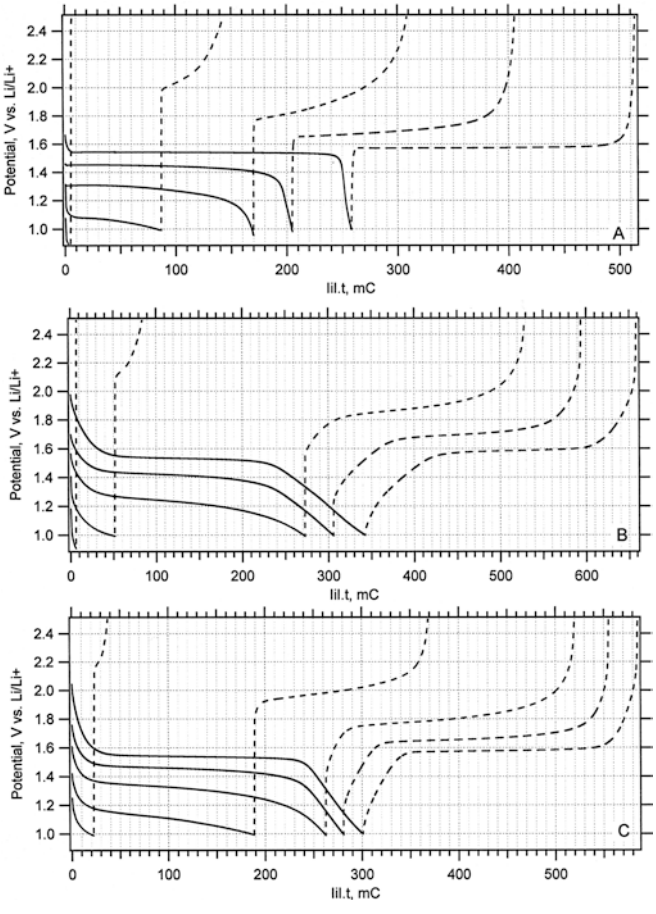

Fig. 5 Chronopotentiometric plot of (A) a commercial $Li_4Ti_5O_{12}$ spinel (LT-2), (B) nanocrystalline $Li_4Ti_5O_{12}$ without hydrothermal treatment and (C) hydrothermally grown nanocrystalline $Li_4Ti_5O_{12}$. Electrolyte solution: 1 M $LiN(CF_3SO_2)_2$ + EC/DME (1:1 by mass). The current *i* was adjusted to a charging rate of 2, 20, 50, 100 and 150 C for the *solid curves* from *top to bottom*. The *dashed curves* display the corresponding galvanostatic discharging at the same rates. For the sake of clarity, the time (*t*) is multiplied by the absolute value of the charging/discharging current, *i*

electrolyte solution, such as reduction of trace water, which is more pronounced for high-surface-area electrodes and for fresh electrodes during the initial cycles (to minimize the second effect, we have pretreated the virgin electrodes by several charging/discharging cycles). Although we did not test the cycle life systematically in long-term experiments, there were no signs of capacity fading during the initial ca. 10 cycles.

The plots in Fig. 5 can be referred to those presented previously for non-optimized sol-gel spinels [21]. The actual charge capacity of our electrodes (Figs. 4, 5) is about twice as large, which cuts down the charge capability at very fast rates (cf. [21]). The improvement of the charging rate for the nanocrystalline material is clearly expressed if we compare the plot for the microcrystalline LT-2

(Fig. 5A) and the autoclaved nanocrystalline materials (Fig. 5C). The latter sample could be charged to almost 70% of its nominal (2 C) capacity at the 100 C rate.

The as-received (non-autoclaved) nanocrystalline spinel (Fig. 5B) is relatively less efficient at fast charging rates, as compared to the charging performance of the autoclaved sample (Fig. 5C). Since the autoclaved sample has larger particles, this would indicate that the charge capability need not monotonously increase with decreasing particle size. In other words, there seems to be a certain optimum particle size, from which the charge capability drops down in both directions, i.e. for either larger or smaller particles.

However, there are also other factors, besides the particle size, which may play a role. The X-ray diffraction patterns show that the non-autoclaved material exhibits a smaller cubic lattice constant (see above). Autoclaving apparently restores the "normal" (larger) value of the lattice constant, which matches, obviously, the improvement in the rate of Li insertion. The hydrothermal recrystallization causes not only the particle growth, but it can also remove defects of the as-received crystals. The quenching of defects may also be beneficial for Li insertion, although the relations between defects and the Li-insertion rate need not be that straightforward. Still another effect to be considered for ultrasmall particles is the energy of Li^+–Li^+ repulsion, which is known to scale with d^{-3} and which slows down the Li^+ transport in the host lattice [23]. The relative influence of the mentioned effect is difficult to assess, although, qualitatively, they all point at the same conclusion that the hydrothermally recrystallized, medium-sized (in mesoscopic dimensions) particles present the optimum morphology for fast Li insertion in thin-film electrodes.

Acknowledgements This work was supported by NTera Ltd. and by the EC-COST Action D14/0002/99. We thank Estelle De Chambrier (NTera) for the TEM measurements.

References

1. Colbow KM, Dahn JR, Haering RR (1989) J Power Sources 26:397
2. Ferg E, Gummov RJ, de Kock A, Thackeray MM (1994) J Electrochem Soc 141:L147
3. Ohzuku T, Ueda A, Yamamoto N (1995) J Electrochem Soc 142:1431
4. Takai S, Kamata M, Fujine S, Yoneda K, Kanda K, Esaka T (1999) Solid State Ionics 123:165
5. Zaghib K, Simoneau M, Armand M, Gauthier M (1999) J Power Sources 81–82:300
6. Deschanvers A, Raveau B, Sekkal Z (1971) Mater Res Bull 6:699
7. Harrison MR, Edwards PP, Goodenough JB (1985) Philos Mag B 52:679
8. Pyun SI, Kim SW, Shin HC (1999) J Power Sources 81–82:248
9. Scharner S, Weppner W, Schmid-Beurmann P (1999) J Electrochem Soc 146:857
10. Zaghib K, Armand M, Gauthier M (1998) J Electrochem Soc 145:3135
11. Peramunage D, Abraham KM (1998) J Electrochem Soc 145:2609
12. Amatucci GG, Badway F, Du Pasquier A, Zheng T (2001) J Electrochem Soc 148:A930
13. Du Pasquier A, Laforgue A, Simon P, Amatucci GG, Fauvarque JF (2002) J Electrochem Soc 149:A302
14. Kavan L, Grätzel M, Rathousky J, Zukal A (1996) J Electrochem Soc 143:394
15. Kavan L, Attia A, Lenzmann F, Elder SH, Grätzel M (2000) J Electrochem Soc 147:2897
16. Kavan L, Rathousky J, Grätzel M, Shklover V, Zukal A (2000) J Phys Chem B 104:12012
17. Fattachova D, Krtil P (2002) J Electrochem Soc 149:A1224
18. Bach S, Pereira-Ramos JP, Baffier N (1999) J Power Sources 81–82:273
19. Bach S, Pereira-Ramos JP, Baffier N (1998) J Mater Chem 8:251
20. Shen C, Zhang X, Zhou Y, Li H (2002) Mater Chem Phys 78:437
21. Kavan L, Grätzel M (2002) Electrochem Solid-State Lett 5:A39
22. Lei Y, Zhang LD, Fan JC (2001) Chem Phys Lett 338:231
23. Choi YM, Pyun SI (1997) Solid State Ionics 99:173